https://doi.org/10.5194/egusphere-2025-6276
Preprint. Discussion started: 12 February 2026

Revisiting the critical role of stabilized Criegee intermediates (sCIs) in sulfuric acid formation: coupling mechanistic updates with interpretable machine learning

Yuhuan Zhu[1], Qiang Chen[1,2], Luyan He[1], Chunlin Shang[3], Li Jiang[4], Donghong Guan[4], Guirong Yao[4], Wenkai Guo[5]

[1]Key Laboratory for Semi-Arid Climate Change of the Ministry of Education, College of Atmospheric Sciences, Lanzhou University, Lanzhou, 730000, China
[2]Lanzhou University Applied Technology Research Institude Co., Ltd, Lanzhou, 730000, China
[3]Inner Mongolia Autonomous Region Environmental Monitoring Center, Wuhai Branch, Wuhai, 016000, China
[4]Gansu Provincial Ecological and Environmental Engineering Assessment Center, Lanzhou 730000, China
[5]Faculty of Geosciences and Environmental Engineering, Southwest Jiaotong University, Chengdu, 611756, China

Correspondence to: Qiang Chen(chenqqh@lzu.edu.cn)

Abstract. Sulfuric acid (H_2SO_4) is a key driver of atmospheric new particle formation and subsequent growth, playing a critical role in the formation of sulfate aerosols. While stabilized Criegee intermediates (sCIs) are recognized to be one of the free radicals oxidated sulfur dioxide (SO_2), alongside the dominant hydroxyl radical (OH), their role in the formation of H_2SO_4 remains poorly understood due to uncertainties in current chemical mechanisms. Here, we quantify the impact of updated sCIs chemistry within the MCM v3.3.1 mechanism using an XGBoost-SHAP model, revealing that the updated mechanism significantly amplifies the contribution of precursor species to the sCIs oxidation rate by a factor of 1.97−10.75. To identify scenarios where sCIs effectively compete with OH, sensitivity analysis highlights ozone (O_3) and alkenes as the primary synergistic drivers promoting the fractional contribution of sCIs to H_2SO_4 ($\mu_{sCIs\%}$). Furthermore, nitrogen oxides (NO_x) exert a distinct diurnal regulatory effect: lower NO_x levels enhance $\mu_{sCIs\%}$ during the day by limiting OH propagation, whereas high NO_x promotes μsCIs% at night by accelerating OH termination. To assess ambient atmosphere implications, we used a Random Forest model to identify a period where gas-phase pathways dominated sulfate formation. Constrained AtChem simulations demonstrate the updated mechanism elevates sCIs contributions to H_2SO_4 from 1.11% to 7.13% by day and 2.95% to 15.72% by night. These findings underscore the significance of sCIs for H_2SO_4 production, especially in urban environments with high O_3 from imbalanced VOC/NO_x reductions, and under nighttime conditions with low photolysis-dependent OH.

Graphical abstracts.

https://doi.org/10.5194/egusphere-2025-6276
Preprint. Discussion started: 12 February 2026

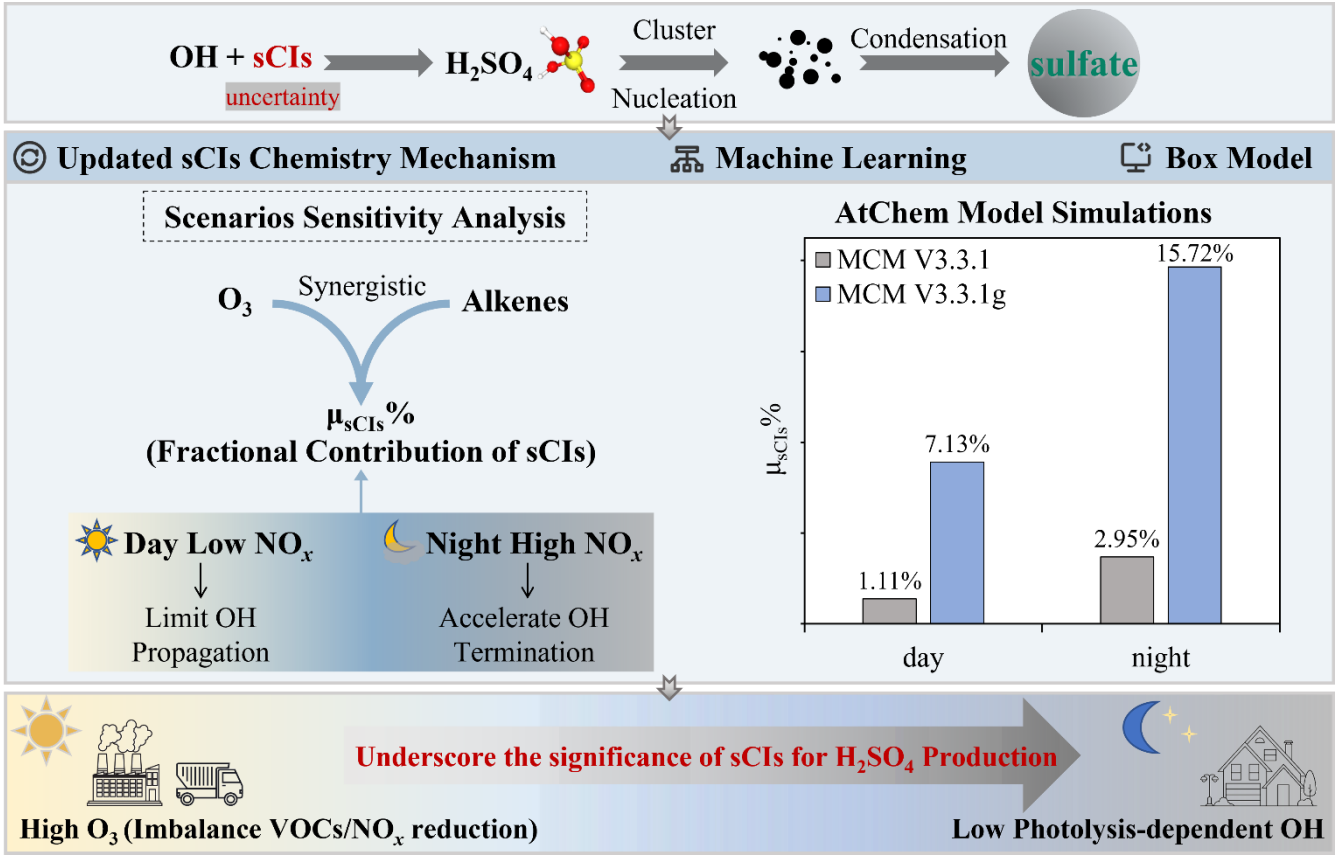

1 Introduction

Fine particles (particles with aerodynamic diameters smaller than 2.5 μm, $PM_{2.5}$) is a significant contributor to globally pressing ecological and environmental challenges, including its role in climate change(Quaas et al., 2022), its harmful effects on air quality(Lyu et al., 2024) and human health(Chen, 2020; Orellano, 2020). The chemical composition of $PM_{2.5}$ strongly shapes its toxicity and radiative forcing(Ren et al., 2021). Sulfate (SO_4^{2-}) is a major constituent of $PM_{2.5}$, attributed to its high concentration ratio and its significant influence on particle hygroscopicity(Gunthe et al., 2011) and clustering behavior(Yao et al., 2018). Sulfate is primarily formed through the gas-phase, aqueous-phase, and heterogeneous-phase oxidation of sulfur dioxide (SO_2)(Ye et al., 2023). Significant sources of sulfate also include the combustion of coal and biomass(Dai et al., 2019) , industrial process emissions(Song et al., 2025) and transportation emissions(Cao et al., 2025). Research efforts to refine the understanding of its complex formation mechanisms near the surface are ongoing. During severe haze events, high humidity and substantial particle loads facilitate the liquid-phase and heterogeneous oxidation of SO_2, making these processes the primary secondary sources of sulfate and, therefore, the focus of extensive mechanistic research(Cao et al., 2021). However, over the past decade, the significant reduction in $PM_{2.5}$ concentrations across developing countries in East

https://doi.org/10.5194/egusphere-2025-6276
Preprint. Discussion started: 12 February 2026

Asia, particularly in China(Geng et al., 2021), driven by air-pollution control measures has diminished the conditions that favor heterogeneous oxidation. Consequently, under higher emission reduction requirements(Anon, 2021), the gas-phase pathway may require more attention in the formation of sulfate(Wang et al., 2025).

The gas-phase formation of sulfate involves the oxidation of SO_2 by hydroxyl radicals (OH) and stabilized Criegee intermediates(sCIs) to produce gaseous sulfuric acid (H_2SO_4), which subsequently condenses and aggregates into atmospheric aerosol particles. While OH-driven oxidation of SO_2 typically dominates H_2SO_4 production, recent studies show that sCIs can provide a significant competing source under certain conditions(Anon, n.d.). Atmospheric observations from a boreal forest region in Finland, supported by laboratory experiments and theoretical analyses, demonstrate that incorporating sCIs oxidation reactions significantly improves the agreement between measured and calculated H_2SO_4 concentrations. This finding suggests that the reaction of sCIs with SO_2 could contribute as much as 33–46% to atmospheric H_2SO_4 concentrations at ground level (Boy et al., 2013). Proxy calculations of H_2SO_4 concentrations reveal that the contributions of OH and sCIs are 0.34 and 0.6, respectively, in a semi-pristine boreal forest, compared to 0.28 and 0.22 in a heavily polluted megacity(Dada et al., 2020). During a continuous observation campaign in Beijing during winter, it was found that nighttime H_2SO_4(g) production under clean conditions showed a strong correlation with the $[SO_2][O_3]$[alkene] source term(Guo et al., 2021a). Existing studies have reported significant contributions of sCIs to H_2SO_4 formation in both urban and forest (including rainforest) environments. In some regions or under specific conditions, sCIs can play a role comparable to that of OH(Shabin et al., 2023).

The cyclo-addition reaction between ozone and alkenes produces energy-rich primary ozonide (POZ), which rapidly decomposes into carbonyl compounds and Criegee intermediates (CIs) (Criegee et al., 1954). The decomposition reaction is exothermic, resulting in excess energy distributed within the CIs. These CIs subsequently undergo either unimolecular decomposition or collisions with other gas molecules, forming sCIs. Like CIs, some sCIs undergo unimolecular decomposition as well, resulting in the formation of OH radicals and other free radicals. The remaining sCIs participate in bimolecular reactions with molecules such as SO_2, NO_x, H_2O, and water dimer ($(H_2O)_2$)(Khan et al., 2018). The evolution of sCIs is highly sensitive to the structure of alkenes. Due to the intense competition between $H_2O/(H_2O)_2$ and SO_2 for reaction with sCIs(Newland et al., 2015a), the oxidation of SO_2 by sCIs is more favored under low-humidity conditions, which is concurrently the regime where gas-phase SO_4^{2-} formation dominates. Alkenes and ozone are the precursors for the formation of sCIs. During the daytime, when photochemical reactions are active, O_3 is primarily formed through reactions between VOCs (including alkenes) and NO_x(Wang et al., 2022a), and subsequently acts as an oxidant, reacting with alkenes to generate sCIs. Meanwhile, OH radicals are produced through the photolysis of precursors such as HONO and, after oxidizing VOCs, are regenerated in the RO_x cycle(Li et al., 2021). At night, O_3 is supplied primarily through enhanced transport and atmospheric mixing, whereas OH is produced mainly via alkene ozonolysis and RO_x cycling. OH and sCIs are intermediate products generated via different reaction pathways, and exhibit complex, nonlinear dependencies on their respective precursors(Zhu et al., 2023). Variations in their relative contributions to the gas-phase oxidation of SO_2 may lead to differences in the relationship between H_2SO_4 formation and its precursors (e.g., VOCs and NO_x). Previous studies on the

https://doi.org/10.5194/egusphere-2025-6276
Preprint. Discussion started: 12 February 2026

contribution of sCIs to H_2SO_4 formation have primarily focused on environments characterized by high alkene concentrations and a particular emphasis on the impact of biogenic emissions(Kukui et al., 2021). However, due to disproportionate pollutant emission reductions(Tang et al., 2025), a more complex air pollution landscape has emerged in some industrial cities(Ye et al., 2025): not only do VOCs concentrations remain elevated, but the frequency of O_3 pollution events has shown no significant downward trend, often accompanied by $PM_{2.5}$ complex pollution(Zhu et al., 2023). Consequently, systematic assessments of the importance of sCIs under different environmental conditions are still lacking, and the key mechanisms that determine their influence on H_2SO_4 remain unclear.

Here, we updated the reaction kinetics of sCIs within the Master Chemical Mechanism (MCM v3.3.1) using the latest research findings, thereby minimizing kinetic uncertainties. A comparative analysis was conducted to assess the oxidation rates of sCIs before and after the mechanism update, identifying the key species that enhance oxidation capacity. Given that sCIs and OH radicals share key precursors and function as secondary oxidants, we investigated the fractional contribution of sCIs to H_2SO_4 production under diverse pollution scenarios to define the specific regimes where sCIs effectively compete with OH. Through mechanistic analysis, we elucidated the critical pathways determining the oxidative role of sCIs. To validate these results in the ambient atmosphere lacking direct H_2SO_4 observations, we utilized a Random Forest (RF) model to screen for a representative episode characterized by gas-phase-dominated SO_4^{2-} formation. Constrained simulations were performed using the AtChem box model to quantify the contribution of sCIs to H_2SO_4 and to discuss the impact of their fractional contribution on SO_4^{2-} sensitivity to its precursors.

2 Data and methodology

2.1 Updating the sCIs gas-phase chemical mechanism

The parameters of the CIs evolution process include the ozonolysis reaction rate coefficient of alkenes (k_i), OH yield ($Y_{i,OH}$), sCIs yield ($Y_{i,sCI}$), sCIs unimolecular decomposition rate ($k_{i,d}$), and bimolecular reaction rate coefficient ($k_{i,b}$). MCM v3.3.1 is a near-explicit chemical mechanism that provides a detailed representation of the generation, loss, and subsequent evolution of Cls. However, the relevant reaction parameters have not been updated to the latest research results, and critical processes such as unimolecular decomposition and reactions with water dimers are neglected. Rate coefficients for the reactions of O3 with alkenes and the reaction mechanisms in MCM v3.3.1 follow recommendations that have been reviewed by Jenkin(Jenkin et al., 2015) and Saunder(Saunders et al., 2003). Previous studies have shown that C1-C4 alkenes contributes more than 85% to sCIs, which are predicted to be among the most important sCIs in tropospheric chemistry(Cox et al., 2020). We used the suggested data provided by (Cox et al., 2020) to update the gas-phase chemical mechanism of O_3+alkenes systems in MCM v3.3.1. The reaction of sCIs and bimolecular water were added, where the concentration of bimolecular water is 10^4 times the concentration of H_2O in the atmosphere. The original parameters and the updated values of sCIs' bimolecular reactions are shown in Table 1. The original parameters and the updated values of $Y_{i,OH}$ and $Y_{i,sCI}$ are shown in Table 2. Detailed information about mechanism update is presented in Table S1.

https://doi.org/10.5194/egusphere-2025-6276
Preprint. Discussion started: 12 February 2026

Table 1. Comparison of rate coefficients of sCIs' bimolecular reactions before and after update.

sCIs	$k_{(sCIs+SO2)}$	$k_{(sCIs+H2O)}$	$k_{(sCIs+(H2O)2)}$	$k_{(sCIs+NO)}$	$k_{(sCIs+NO2)}$	$k_{(sCIs+M)}$	reference
CH2OO	3.7×10^{-11}	2.8×10^{-16}	6.4×10^{-12}	$< 6\times10^{-14}$	3×10^{-12}	$\leq 2\times10^{-1}\ s^{-1}$	MCM v3.3.1g
	7.0×10^{-14}	1.0×10^{-17}	/	1.0×10^{-14}	1.0×10^{-15}	/	MCM v3.3.1
E-CH3CHOO	1.4×10^{-10}	1.3×10^{-14}	4.4×10^{-11}	/	2.0×10^{-12}	6.0×10^{1}	MCM v3.3.1g
	7.0×10^{-14}	1.0×10^{-17}	/	1.0×10^{-14}	1.0×10^{-15}	/	MCM v3.3.1
(CH3)2COO	1.55×10^{-10}	$< 1.5\times10^{-16}$	$< 1.3\times10^{-13}$	/	2.1×10^{-12}	4.0×10^{2}	MCM v3.3.1g
	7.0×10^{-14}	6.0×10^{-18}	/	1.0×10^{-14}	1.0×10^{-15}	/	MCM v3.3.1
E-(CH=CH2)(CH3)COO	4.2×10^{-11}	7.89×10^{-20}	3.06×10^{-16}	/	/	5.13×10^{1}	MCM v3.3.1g
	7.0×10^{-14}	6.0×10^{-18}	/	1.0×10^{-14}	1.0×10^{-15}	/	MCM v3.3.1
E-(C(CH3)=CH2)CHOO	1.4×10^{-10}	1.43×10^{-16}	2.79×10^{-13}	/	/	3.02×10^{1}	MCM v3.3.1g
	7.0×10^{-14}	1.0×10^{-17}	/	1.0×10^{-14}	1.0×10^{-15}	/	MCM v3.3.1

Table 2. Comparison of rate coefficients of $Y_{i,OH}$ and $Y_{i,sCI}$ before and after update.

alkene	$Y_{i,sCI}$	$Y_{i,OH}$	reference
ethene	0.42	0.17	MCM v3.3.1g
	0.37	0.13	MCM v3.3.1
propene	0.28	0.36	MCM v3.3.1g
	0.24	0.36	MCM v3.3.1
but-1-ene	0.23	0.38	MCM v3.3.1g
	0.24	0.36	MCM v3.3.1
cis-but-2-ene	0.20	0.33	MCM v3.3.1g
	0.18	0.57	MCM v3.3.1
trans-but-2-ene	0.22	0.60	MCM v3.3.1g
	0.18	0.57	MCM v3.3.1
2-methylpropene	0.20	0.67	MCM v3.3.1g
	0.18	0.82	MCM v3.3.1
isoprene	0.66	0.26	MCM v3.3.1g
	0.56	0.25	MCM v3.3.1

2.2 Model setup and observation data

2.2.1 Model setup

AtChem v1 (an open-source box model for MCM v3.3.1) was used to simulate the gas-phase reaction pathways by which sCI and OH oxidize SO2 to SO3. The updated mechanism, MCM v3.3.1g, was integrated into the AtChem model. The model was constrained by the observed meteorological parameters (T, RH, and P), J(NO_2), and trace gases (NO_x, CO, SO_2, HONO, NMHCs, OVOCs, and PAN). L_{SO2}(g) represents the total gas phase oxidation rate of SO_2. $L_{SO2,sCIs}$(g) and $L_{SO2,OH}$(g)

https://doi.org/10.5194/egusphere-2025-6276
Preprint. Discussion started: 12 February 2026

are used to indicate the rate of SO_2 gas phase oxidation by sCIs and OH, respectively. sCIs% denotes the contribution of sCIs to the total gas-phase oxidation rate of SO_2.

2.2.2 Observation data

All hourly data from the automatic monitoring system at the Wuhai City Atmospheric Environment Super Monitoring Station for the period from September 1, 2019 through June 2022. The dataset includes air pollutants ($PM_{2.5}$, carbon monoxide (CO), sulfur dioxide (SO_2), nitrogen dioxide (NO_2), ozone (O_3)); meteorological variables (wind speed (WS), wind direction (WD), temperature (T), pressure (P), relative humidity (RH)); ion species (Cl^-, NH_4^+, NO_3^-, SO_4^{2-}, etc.); and elemental species (Mn, Fe, etc.). $PM_{2.5}$, NO_2, SO_2, CO, and O_3 were measured with a Metone BAM-1020 $PM_{2.5}$ Monitor, an API T201 NH_3-NO_x Analyzer, an API T100 SO_2 Analyzer, an API T300 CO Analyzer, and an API T400 O_3 Analyzer, respectively. VOCs were measured using an ENTECH BCT-7800 VOCs Analyzer. Ion data were obtained with a Metrohm MARGA ADI 2080 online ion chromatograph. Elements (Na, Fe, Ni, K, etc.) were determined with a CES Xact-625 atmospheric heavy metal analyzer. Meteorological variables (T, RH, P, WS, WD) were measured with a six-parameter meteorological sensor (Lufft WS601-UMB). Photolysis rate coefficients, including $J(O^1D)$ and $J(NO_2)$, etc, were measured with a Metcon UF-CCD Photolysis Spectroradiometer.

2.3 Machine learning method

In this study, we treated the AtChem inputs as features and the outputs as target variables and trained Extreme Gradient Boosting (XGBoost) and Random Forest (RF) models. We interpreted the model results using analysis of variance (ANOVA), partial dependence plots (PDPs), and shapley additive explanations (SHAP).

2.3.1 XGBoost and RF Model

Extreme gradient boosting (XGBoost) is a gradient-boosting-based ensemble algorithm that improves traditional techniques with remarkable attributes, including efficiency, precision, stability, and scalability(Fatahi et al., 2022). It builds an ensemble of decision trees in a sequential manner, where each tree corrects the errors of the previous one by minimizing a specified loss function. The model incorporates regularization techniques, such as L1 and L2 penalties, to prevent overfitting and improve generalization. In this study, the XGBoost model was implemented using the Python xgboost library. Key hyperparameters were optimized through grid search and cross-validation.

Random Forest (RF) is a canonical ensemble learning algorithm composed of decision trees as base learners, proposed by Breiman in 2001(Breiman, 2001), and used for both classification and regression tasks. Compared with other machine learning models, RF offers advantages in training speed, predictive accuracy, and ease of use, and has been widely applied in researches(Wang et al., 2022b).

https://doi.org/10.5194/egusphere-2025-6276
Preprint. Discussion started: 12 February 2026

2.3.2 Model interpretation

PDP shows the dependence of one or two features on the predicted results of the machine learning models(Friedman, 2001). x_i represents a set containing only one features, x_c is the set of other features. The features in set i are those that this study focuses on to reveal their impact on the prediction results. x_i and x_c constitute the total features and are used as input features for the model. f is the XGBoost model.

$$f_{x_i}(x_i) = Ex_c[f(x_i, x_c)], \quad (1)$$

SHAP(Lundberg et al., 2018) is a method grounded in cooperative game theory, which was originally used to allocate a total payoff among players. By analogy, each feature in a dataset can be viewed as a "player," and the model prediction obtained after training on the dataset can be regarded as the cooperative payoff produced by these players working together. Shapley values fairly distribute this payoff by accounting for each player's contribution; in other words, they quantify the contribution of each feature to each individual prediction. Global feature effects are assessed with the SHAP summary(beeswarm), feature-importance, and dependence plots, while local interpretability for individual predictions is provided by the waterfall plot. SHAP has been widely adopted across a broad range of fields(Chen et al., 2024; Yi and Wu, 2023). In this study, the SHAP analysis was conducted to identify important features(Li et al., 2023; Liu et al., 2025) and explore interactions between factors and target variables.

3 Results and Discussion

3.1 Impact of the Mechanism Update on Key Drivers of $L_{SO2,sCIs}(g)$

$L_{SO2,sCIs}(g)$ is determined by the type of alkenes, the concentration levels of alkenes, O_3, and H_2O, as well as all reaction parameters related to the evolution of CIs. In order to further elucidate the contribution of each reactant to $L_{SO2,sCIs}(g)$ and to understand the uncertainty caused by the reaction parameters, we classified humidity (RH), cis-2-butene(CBUT2ENE), trans-2-butene (TBUT2ENE), ozone (O_3), isoprene (C5H8), Isobutene (MEPROPENE), propylene/butene (C3C4), ethylene (C2H4) are selected as the main species that contribute significantly to the sCIs-mediated gas-phase oxidation of SO_2. We used $L_{SO2,sCIs}(g)$, obtained from AtChem coupled with either MCM v3.3.1 or MCM v3.3.1g, as the target variable. Concentrations of the main species served as features and were fed into an XGBoost model, with SHAP used for interpretation.

Using an XGBoost-based SHAP analysis, we computed SHAP values for feature sets from the pre- and post-revision mechanisms and identified the key features driving sCIs oxidative capacity. Figures 1a and 1b displays the global SHAP values for each feature, ranked from top to bottom by their mean |SHAP| values. The positive/negative association of each feature with $L_{SO2,sCIs}(g)$ didn't change between mechanisms. As shown in Figs. 1a, 1b, low relative humidity (blue points) corresponds to positive SHAP values, whereas high relative humidity (red points) corresponds to negative SHAP values,

https://doi.org/10.5194/egusphere-2025-6276
Preprint. Discussion started: 12 February 2026

consistent with previous studies(Newland et al., 2015b), indicating that humidity exerts a negative contribution to $L_{SO2,sCIs}(g)$. This occurs because higher $H_2O/(H_2O)_2$ concentrations compete more effectively with SO_2 for reacting with sCIs, reducing the amount of sCIs available to oxidize SO_2. It is well established that under humid conditions, sulfate (SO_4^{2-}) production is dominated by the aqueous-phase oxidation of SO_2, not only because humidity alters the relevant phase state, but also because $H_2O/(H_2O)_2$ efficiently scavenges sCIs. Other drivers, such as O_3 and alkenes, show positive associations with $L_{SO2,sCIs}(g)$. However, the magnitudes of these features' contributions to $L_{SO2,sCIs}(g)$ differ significantly before and after the mechanism modification (Figs. 1c, 1d). When using the MCM v3.3.1 mechanism, the average contribution range of each factor was 517.16–10522.46 mole·cm^{-3}·s^{-1}, which increased several-fold to 2390.64–37718.57 mole·cm^{-3}·s^{-1} with the MCM v3.3.1g mechanism (Fig. 1c). Furthermore, significant differences were observed in the magnitude of change in these key components' contributions to the $L_{SO2,sCIs}(g)$ before and after the mechanism update (Fig. 1c). When using the MCM v3.3.1 mechanism, the ranking of factor importance was as follows: trans-2-butene (26%) > RH (25%) > cis-2-butene (18%) > O_3 (17%) > isoprene (9%) > isobutene (3%) > propylene/butene (1.5%) > ethylene (1.4%). After the mechanism update, the order of factor importance changed to: isoprene (26%) > O_3(20.4%) > RH (19.8%) > trans-2-butene (15%) > cis-2-butene (10%) > isobutene (4.4%) > propylene/butene (3.1%) > ethylene (1.5%) (Fig. 1d). Among them, isoprene exhibited the most significant variation compared to other alkenes, with its average SHAP value changing from 3507.93 mole·cm^{-3}·s^{-1} (contributing approximately 9%) with MCM v3.3.1 to 37718.57 mole·cm^{-3}·s^{-1} (contributing approximately 26%) with MCM v3.3.1g. This finding is consistent with results from previous studies(Hata et al., 2023; Newland et al., 2015b) and highlights the importance of isoprene in $L_{SO2,sCIs}(g)$. After the mechanism update, the contributions of O_3 and isobutene to $L_{SO2,sCIs}(g)$ increased, while the relative importance of RH, cis-2-butene, and trans-2-butene declined. The differing changes in alkenes' contributions arise because MCM v3.3.1g explicitly accounts for structure-specific effects on sCIs yields and reaction rate coefficients. In particular, $k_{(sCIs+H2O/(H2O)2)}$ are highly structure-sensitive: greater alkyl branching lowers reactivity toward water. Accordingly, the E-CH3CHOO and CH2OO Criegee intermediates formed from propene and ethene ozonolysis exhibit among the largest rate constants for reactions with H_2O and with the water dimer $(H_2O)_2$. The wider the distribution range of a feature's SHAP values, the stronger its interaction with other features. We found that after modifying the mechanism, the SHAP value distribution range of all alkenes increased to varying magnitudes, which was primarily attributed to the update of $k_{(sCIs+SO2)}/k_{(sCIs+H2O/(H2O)2)}$. This highlights the uncertainty introduced by $k_{(sCIs+H2O/(H2O)2)}$ in the evaluation of $L_{SO2,sCIs}(g)$, consistent with findings reported in a previous study(Liu et al., 2019).

https://doi.org/10.5194/egusphere-2025-6276
Preprint. Discussion started: 12 February 2026

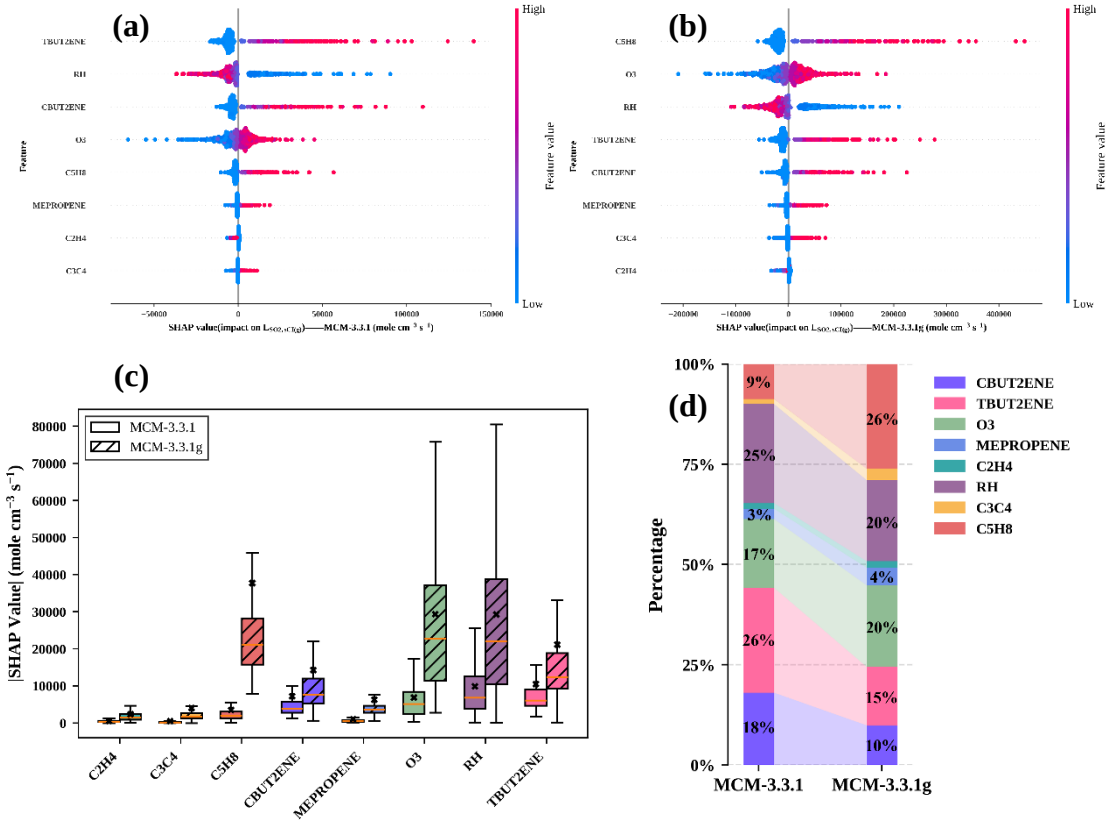

Figure 1. SHAP values calculated based on the XGBoost-SHAP model. The SHAP summary plot in (a) and (b) represent the global SHAP values for all samples MCM v3.3.1 and MCM v3.3.1g respectively, the color change of the scatter plot from blue to red indicates an increase in factor values. The boxplots in (c) represent the |SHAP| values of each key component with MCM v3.3.1 and MCM v3.3.1g respectively. (d) Representation of the relative contribution of SHAP values of each key component before and after the mechanism update.

Figure 2 provides a clearer, more intuitive view of the interaction between alkenes and humidity. When RH is below 20%, alkenes make a positive contribution to $L_{SO2,sCIs}(g)$. As humidity increases, the negative effect of RH increasingly counteracts the positive effect of alkenes; at RH of 30–40%, the positive contribution of alkenes is markedly weakened and may even become slightly negative. Under high humidity (≥50%), the antagonistic effect of RH strengthens further, such that increasing alkene concentrations actually lead to a pronounced decrease in $L_{SO2,sCIs}(g)$. By comparing how the SHAP values of individual alkenes vary with RH, we find that propene and ethene exhibit larger declines than the other alkenes, indicating a stronger antagonistic (inhibitory) effect of relative humidity on these species. Across humidity regimes, the mechanism update increases, to varying degrees, the sensitivity of $L_{SO2,sCIs}(g)$ to changes in alkene concentrations. This behavior is consistent with concurrent increases in the rate coefficients $k_{(sCIs+SO2)}$ and $k_{(sCIs+H2O/(H2O)2)}$.

https://doi.org/10.5194/egusphere-2025-6276
Preprint. Discussion started: 12 February 2026

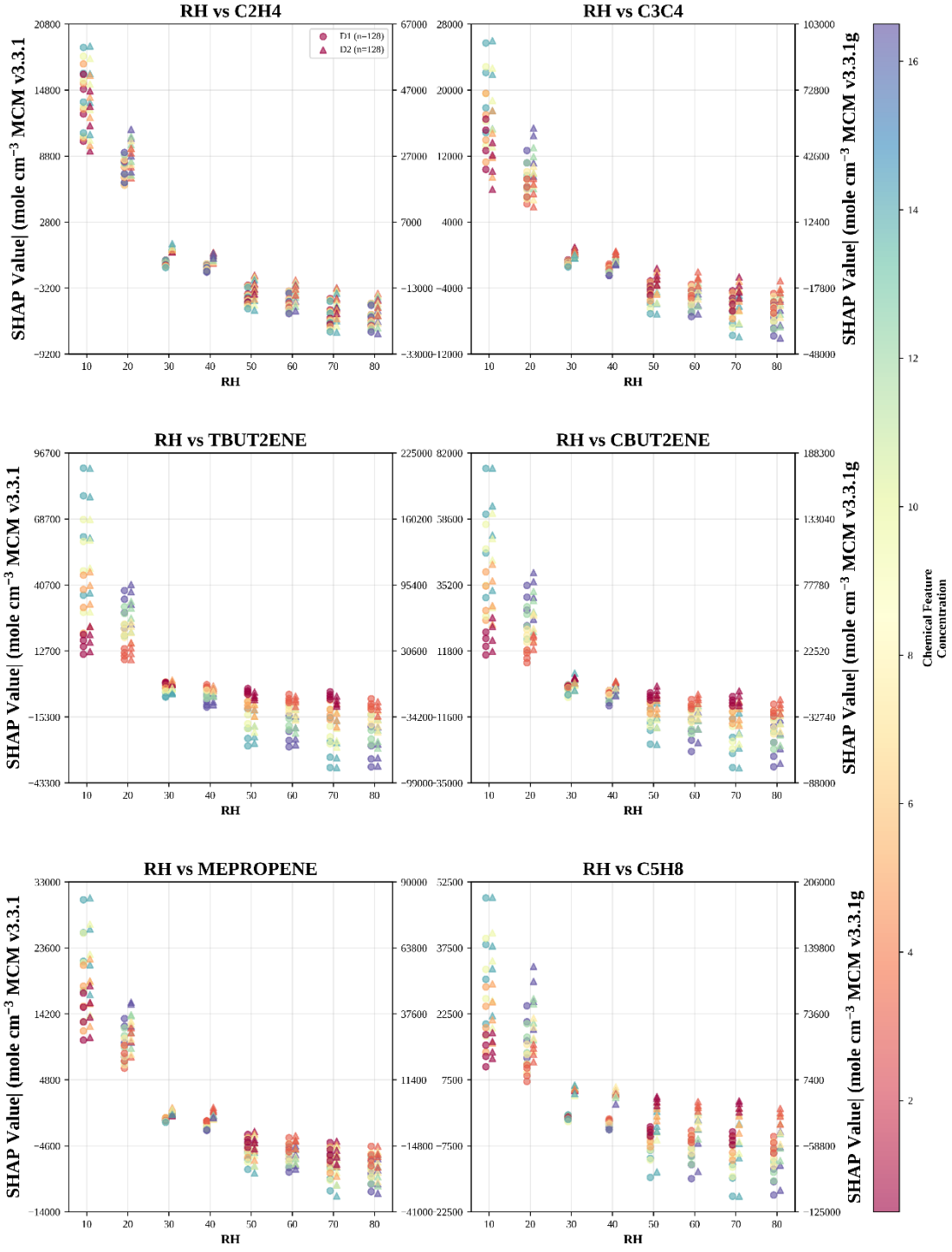

Figure 2. Comparison of the RH dependency of key components (trans-2-butene, cis-2-butene, isoprene, and isobutene) before and after the mechanism update.

https://doi.org/10.5194/egusphere-2025-6276
Preprint. Discussion started: 12 February 2026

3.2 Evaluation of the importance of sCIs in the gas-phase oxidation of SO_2(L_{SO2}(g))

The findings reported in Sect. 3.1 has better demonstrated the high sensitivity of sCIs' oxidation capacity to alkenes and O_3(Guo et al., 2021b). O_3 is primarily formed through a series of complex photochemical reactions involving primary pollutants such as NO_x and VOCs during daytime, with a smaller contribution from vertical transport from the stratosphere. Therefore, it is recognized that sCIs are significantly influenced by both typical primary pollutants (alkenes) and secondary pollutants (O_3) in the atmosphere, while their reaction pathways are simultaneously accompanied by the generation of OH radicals. The complex and highly coupled reactions make the role of sCIs in atmospheric oxidation unclear, leading to a challenging relationship between the oxidation product H_2SO_4 and its precursor. The atmospheric chemical and physical processes of ozone at night differ from those during the day due to the absence of sunlight, which results in minimal secondary formation sources for ozone. Physical processes such as horizontal transport, vertical mixing, local circulation, and stratospheric intrusion are the primary sources of O_3 at night.

In a specific region, the three-year average concentrations of relevant species at each time point served as the baseline. A full factorial, three-level design was applied to five features—NO_x, NO_2% (the NO_2 fraction in NO_x), VOCs, alkene%, and O_3—yielding 243 simulation scenarios. The perturbation levels were set at 10%, 100%, and 190% of the baseline values, which are coded as -1, 0, and 1, respectively, in the subsequent analysis. The target variables were defined as the average sCIs%($\mu_{sCIs\%}$) during daytime (10:00–17:00, UTC+8) and nighttime (22:00–05:00, UTC+8). The relationship between $\mu_{sCIs\%}$ and the five features was modeled using the XGBoost algorithm.

Figure 3a shows that during daytime, the sensitivity relationship between $\mu_{sCIs\%}$ and five variables in modified mechanisms. The three factors with the largest main effects on $\mu_{sCIs\%}$ were O_3, alkene%, and VOCs, in the order O_3 > alkene% > VOCs. Among the second-order interactions, the three strongest pairs all involved O_3, VOCs, and alkene%, namely O_3 × alkene%, O_3 × VOCs, and VOCs × alkene%, each exhibiting statistically significant synergistic effects on $\mu_{sCIs\%}$. By contrast, NO_2% showed a relatively weak main effect with a broad distribution of effect sizes and higher variability. The main effect of NO_x was the weakest; however, its interaction with NO_2% was pronounced. Although NO_x and NO_2% each also interacted with the other three factors, these interactions were weaker than NO_x × NO_2% (Fig. 3a). The relatively strong NO_x × NO_2% interaction indicates that the role of NO_x is conditional, depending on the levels of NO_2% and related factors. It is noteworthy that all interactions between NO_x and the other factors were negative, indicating antagonistic effects. When NO_x levels were low, its inhibitory influence weakened and the positive contributions of other factors to $\mu_{sCIs\%}$ became more apparent, whereas under high NO_x conditions, inhibition strengthened and the positive effects of other factors were suppressed. Consequently, the impact of O_3, VOCs, and alkene% on $\mu_{sCIs\%}$ was impacted on the NO_x concentration.

https://doi.org/10.5194/egusphere-2025-6276
Preprint. Discussion started: 12 February 2026

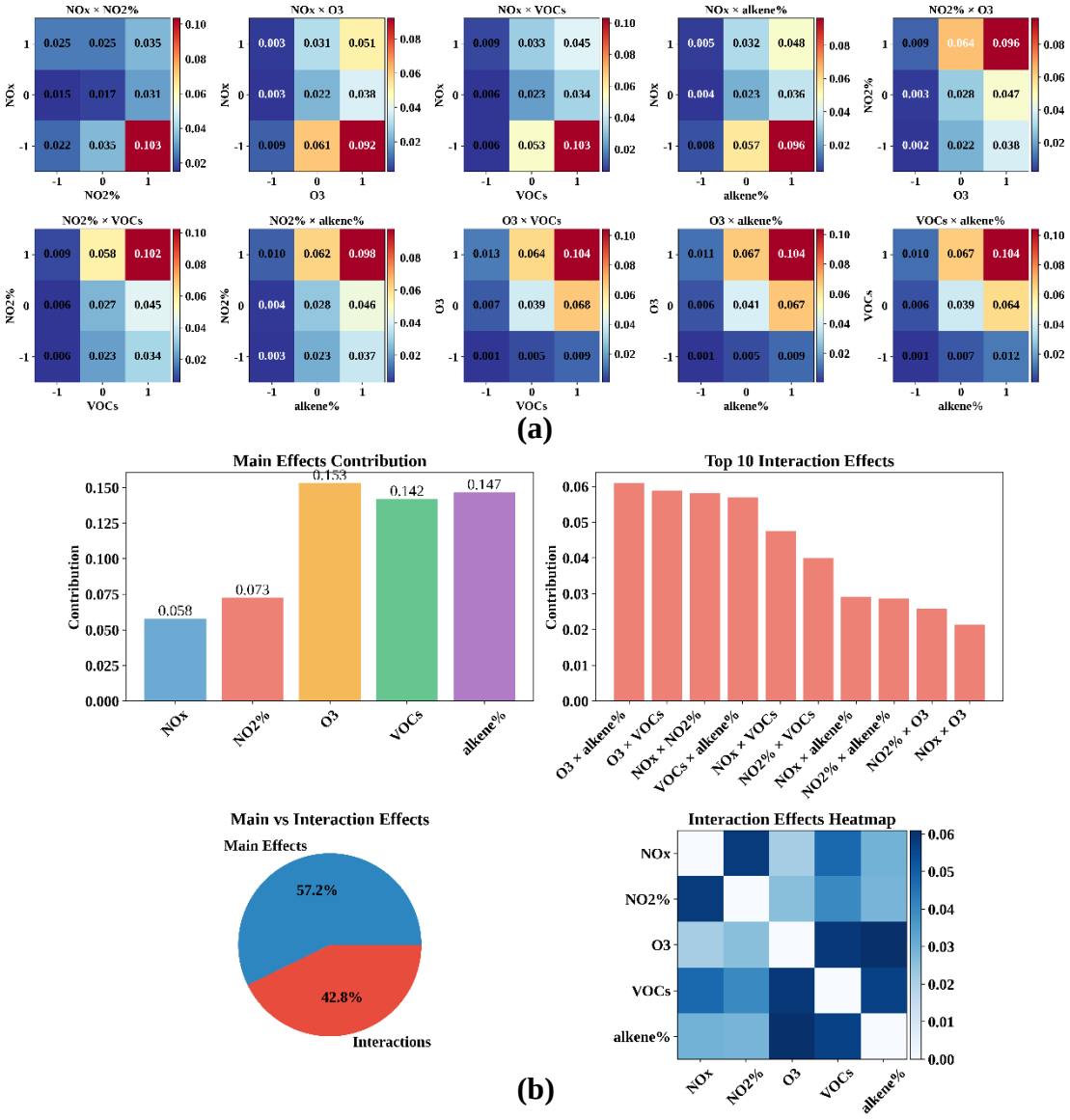

Figure 3. Assessing the role of sCIs in $L_{SO2}(g)$ under daytime pollution scenarios. (a) Two-dimensional interaction partial dependence plots for all features. (b) ANOVA effect analysis for all features.

Figure 4a shows that during nighttime, the sensitivity relationship between $\mu_{sCIs\%}$ and five variables in modified mechanisms. The three factors with the largest main effects on $\mu_{sCIs\%}$ were O_3, alkene%, and VOCs, in the order O_3 > alkene% > VOCs. Among the second-order interactions, the three strongest pairs all involved O_3, VOCs, and alkene%, namely O_3× alkene%, O_3 × VOCs, and VOCs × alkene%, each exhibiting statistically significant synergistic effects on $\mu_{sCIs\%}$. By contrast, NO_x showed a relatively weak main effect and the main effect of NO_2% was the weakest; however, its interaction NO_x × NO_2% was pronounced. NO_x exhibited interactions with each of the other three factors. In contrast to daytime behavior, the

https://doi.org/10.5194/egusphere-2025-6276
Preprint. Discussion started: 12 February 2026

nighttime interactions of NO_x were uniformly positive: at high NO_x, the promoting potential of O_3, VOCs, and alkene% on $\mu_{sCIs\%}$ was unlocked. However, NO_2% displayed an antagonistic interaction with NO_x. Its main effect was negligible, whereas its interaction effect was strong, indicating a conditional role governed by the level of NO_x. When NO_x was large, NO_2% contributed slightly negatively to $\mu_{sCIs\%}$. Correspondingly, when NO_2% was low, its inhibitory influence weakened and the promoting effect of NO_x became more pronounced.

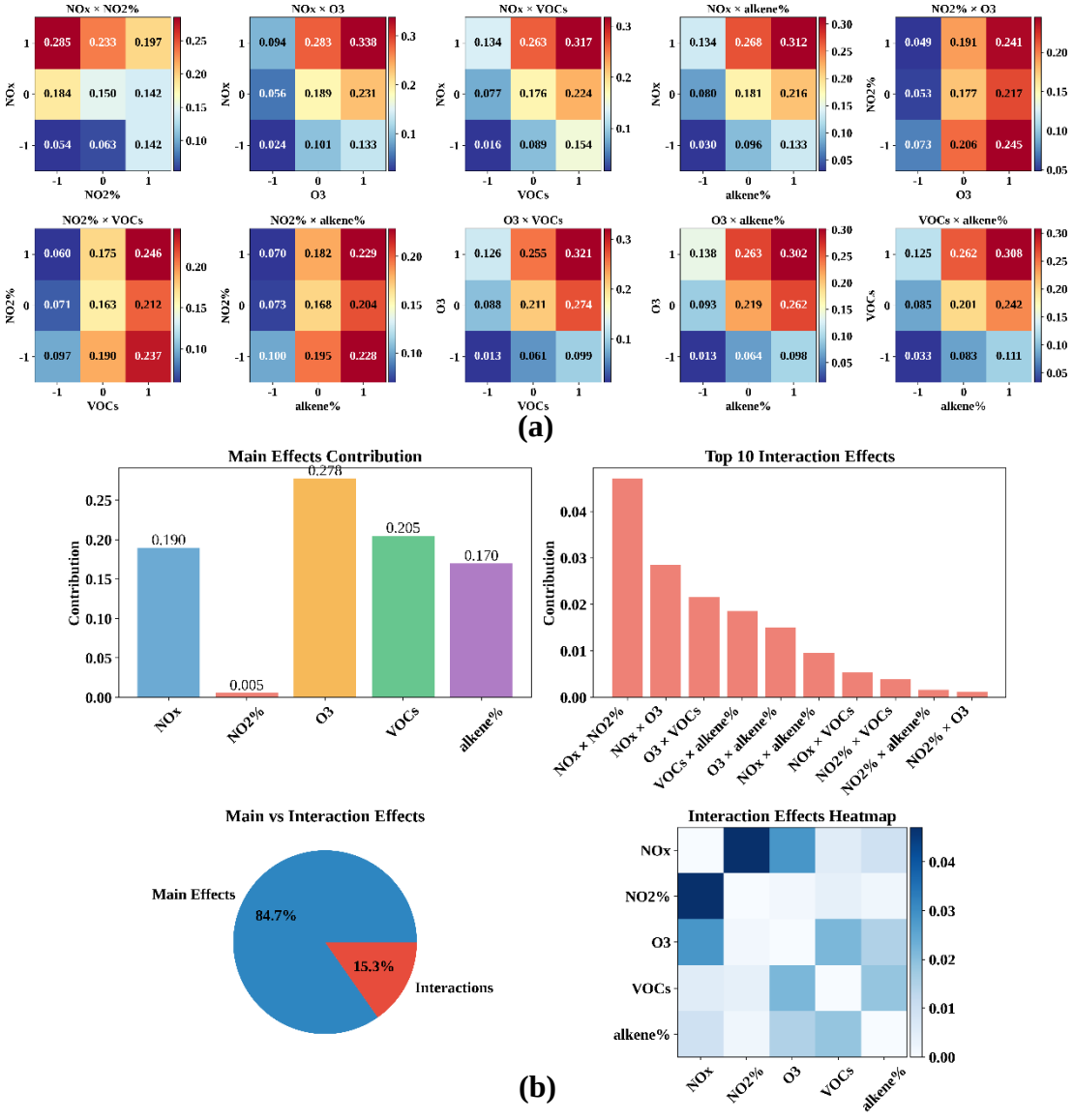

Figure 4. Assessing the role of sCIs in $L_{SO2}(g)$ under nighttime pollution scenarios. (a) Two-dimensional interaction partial dependence plots for all features. (b) ANOVA effect analysis for all features.

https://doi.org/10.5194/egusphere-2025-6276
Preprint. Discussion started: 12 February 2026

During daytime, OH is produced primarily by HONO photolysis, O_3 photolysis, and by radical propagation, whereas its dominant loss is termination with NO_2 forming HNO_3. Because radical propagation proceeds much faster than primary photolysis, the overall pathway is sensitive to the abundance of NO_x and NO_2%. When NOx is low and NO_2% decreases (i.e., NO increases), the HO_2→OH conversion accelerates by a factor of 8.62, net OH production rises, and $L_{SO2,OH}$(g) increases 6.68-fold. Under high NO_x, a low NO_2% already provides sufficient NO to oxidize the available radicals; further increases in NO shift OH toward termination reactions with NO_x, weakening its promoting effect on radical propagation and yielding only a 26% increase in $L_{SO2,OH}$(g) (Table 3). When NO_2% is high but NO_x is low, the newly produced radicals require NO to initiate propagation; increasing NO_x in this regime enhances primary photolytic OH production and markedly strengthens radical cycling, yet abundant NO_2 simultaneously drives OH+NO_2 termination. The net effect is a 2.96-fold increase in $L_{SO2,OH}$(g). Finally, when both NO_2% and NO_x are low, the NO fraction is large and radical cycling approaches saturation; further substantial increases in NO_x cause excess NO_2 to inhibit OH, reducing $L_{SO2,OH}$(g) to 56% of its original value. During the daytime, because radical propagation governs OH concentrations, NO_2% has a greater impact on sCIs% than total NOx, and sCIs% is positively correlated with NO_2% regardless of the NO_x level. The magnitude of NO_2% also determines whether NO_x enhances or suppresses sCIs%.

At night, photolysis is negligible, so OH is supplied only by radical propagation and alkene ozonolysis. Meanwhile, NO_x cycling largely shuts down, and nighttime OH concentrations are far lower than in the daytime. When NO_x is low, an increase in NO accelerates the HO_2→OH conversion, raising $L_{SO2,OH}$(g) by a factor of three; however, because radicals are scarce at night, under high-NO_x conditions, further increases in NO amplify the inhibitory effect of NO_x on OH, leading to a modest decrease in $L_{SO2,OH}$(g) to 0.67 times its previous value. Unlike the daytime, the low radical levels and the fact that HONO (a co-product of NO_x) no longer supplies OH mean that, irrespective of NO_2%, large increases in NO_x tend to divert OH into termination, thereby lowering $L_{SO2,OH}$(g). Consequently, at night the influence of NO2% on sCIs% is weaker than that of NO_x. From the SO_2+sCIs reaction rates in Table 3, neither NO_x nor the NO fraction has a significant effect on $L_{SO2,sCIs}$(g), indicating that their influence on sCIs% occurs primarily through changes in $L_{SO2,OH}$(g).

https://doi.org/10.5194/egusphere-2025-6276
Preprint. Discussion started: 12 February 2026

Table 3. Rates of key reaction pathways under different NO_x-NO_2% scenarios.

	(NO_x, NO_2%)	(-1, 1)	(-1, -1)	(1, 1)	(1, -1)
Reaction rate during daytime ($*10^6$ mole·cm^{-3}·s^{-1})	HONO+hν	0.39	0.39	19.38	19.39
	SO_2+OH	0.25	1.67	0.74	0.93
	NO_2+OH	0.28	0.21	39.60	5.47
	RO_2→HO_2	24.13	207.98	94.26	146.92
	HO_2→OH	40.09	411.82	201.89	300.76
	HO_2 loss	12.95	20.44	0.32	0.01
	NO+O_3	58.43	525.87	2922.47	26306.88
	SO_2+sCIs	0.03	0.04	0.04	0.04
	sCI%	12.27%	2.11%	4.54%	3.66%
Reaction rate during nighttime ($*10^6$ mole·cm^{-3}·s^{-1})	HONO+hν	-	-	-	-
	SO_2+OH	0.11	0.33	0.06	0.04
	NO_2+OH	0.16	0.05	4.06	0.28
	RO_2→HO_2	11.01	34.37	8.40	5.73
	HO_2→OH	16.47	61.79	12.64	8.66
	HO_2 loss	0.80	0.15	0.00	0.00
	NO+O_3	61.15	550.19	3057.29	27515.96
	SO_2+sCIs	0.03	0.03	0.03	0.03
	sCI%	19.71%	7.36%	31.33%	42.80%

Figures 5a, 5b, 5d and 5e illustrate the key reactions that govern the interaction between NO_x and O_3/VOCs. Both during the daytime (Fig. 5c) and at night(Fig. 5f), when NO_x is insufficient, further increases in VOCs promote termination reactions among radicals, thereby lowering OH concentrations. The larger the NO fraction, the smaller the decrease in OH. When NO_x is abundant, increases in VOCs markedly enhance radical cycling, increasing OH concentrations; likewise, a larger NO fraction yields a greater OH increase. The effect of increasing VOCs concentrations on $L_{SO2,sCIs}$(g) is independent of NO_x levels. The increase in $L_{SO2,sCIs}$(g) is nearly commensurate with the increase in VOCs; consequently, VOCs are more effective at enhancing $L_{SO2,sCIs}$(g) relative to their effect on $L_{SO2,OH}$(g).

Overall, O_3 promotes $L_{SO2,OH}$(g) to varying degrees (Fig. 5c). When NO_x is low, increasing O_3 enhances OH production from photolysis but simultaneously strengthens NO-O_3 titration. In this regime, the NO concentration determines how $L_{SO2,OH}$(g) responds: if the NO fraction is high, the HO_2 + NO rate far exceeds the O_3 photolysis rate, and the intensified titration offsets the contribution of O_3 photolysis to OH, leaving OH nearly unchanged; if the NO fraction is low, the impact on titration is smaller than on the photolysis rate, and $L_{SO2,OH}$(g) increases to 1.3 times its previous value. When NO_x is high, regardless of

https://doi.org/10.5194/egusphere-2025-6276
Preprint. Discussion started: 12 February 2026

NO_2%, there is ample NO and O_3 to react, so the strengthened titration has a diminished impact on HO_2+NO; consequently, relative to the (NO_x, NO_2%) = (-1, -1) scenario, $L_{SO2,OH}(g)$ exhibits a larger increase (to 1.09 times). At night (Fig. 5f), O_3 photolysis is negligible, and O_3 affects OH mainly via alkene ozonolysis and titration pathways (Figs. 5d, 5e). Unlike in the daytime, the alkene ozonolysis rate is comparable to the radical cycling rate. Compared with titration, the enhancement of alkene ozonolysis by increasing O3 is stronger, leading to a larger increase in $L_{SO2,OH}(g)$ than during the day. The effect of increasing O_3 concentration on $L_{SO2,sCIs}(g)$ is likewise independent of NO_x. Relative to its effect on $L_{SO2,OH}(g)$, O_3 more effectively enhances $L_{SO2,sCIs}(g)$.

https://doi.org/10.5194/egusphere-2025-6276
Preprint. Discussion started: 12 February 2026

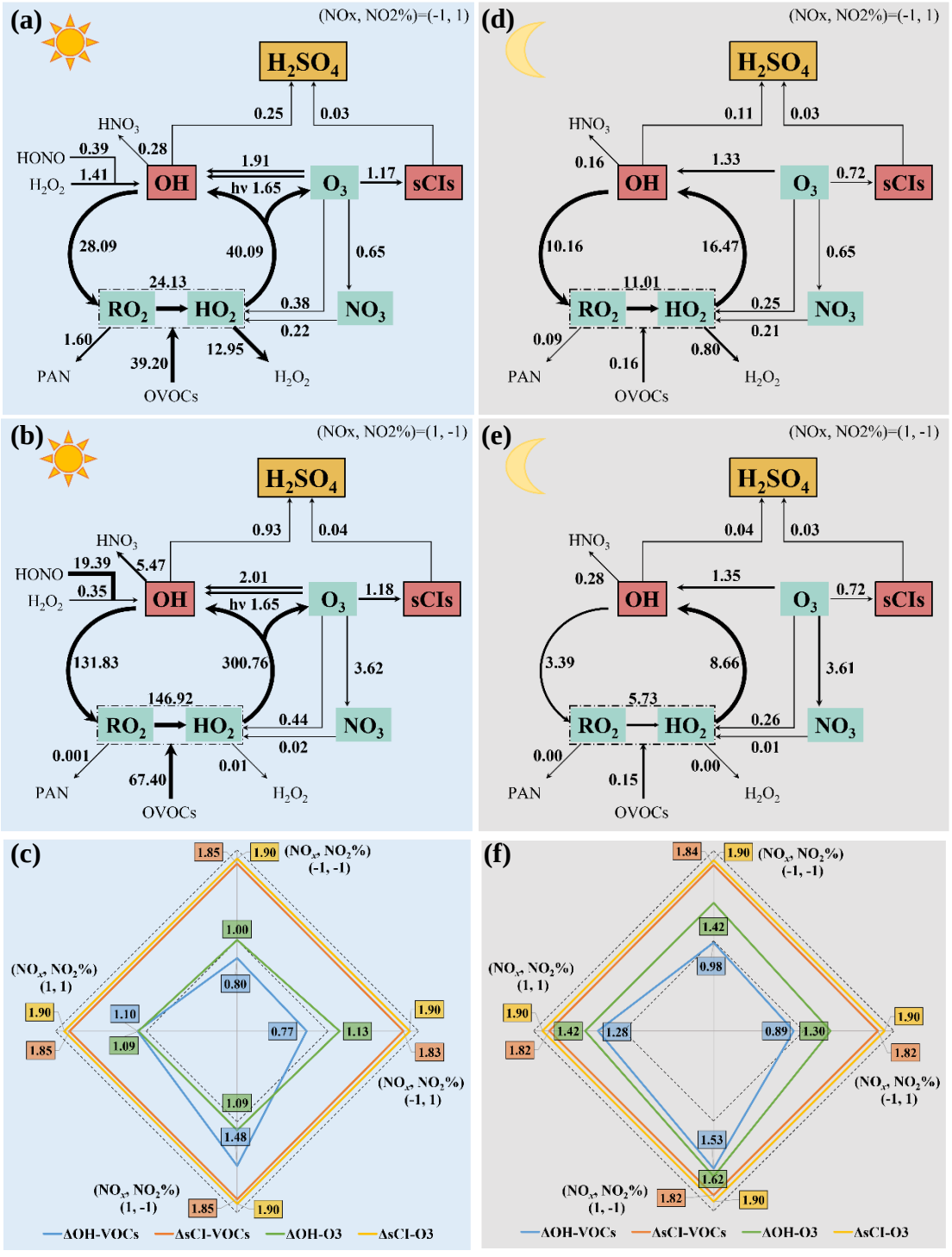

Figure 5. Under different NO_x-NO_2% scenarios: key reaction pathways determining sCIs% during daytime(a, b) and nighttime(d, e); effects of VOCs/O_3 on $L_{SO2,OH}$(g) and $L_{SO2,sCIs}$(g) during daytime(c) and nighttime(f).

https://doi.org/10.5194/egusphere-2025-6276
Preprint. Discussion started: 12 February 2026

3.3 Observation-modeling corroboration of sCIs-driven SO_2 oxidation

Using hourly data from the automatic monitoring system to constrain NO_x, O_3, VOCs, RH, T, P, and photolysis rates, we applied the AtChem model coupled with the MCM v3.3.1 and MCM v3.3.1g mechanisms to simulate the formation of H_2SO_4 during 2021.07.01–2021.07.18. As shown in Fig. 6, after the mechanism was modified, gas-phase sulfuric acid produced via sCIs oxidation (SA-sCIg) increased substantially. During the daytime(10:00-17:00, UTC+8), the average fraction of SA-sCIg in SA-g rose from 1.11% to 7.13%; at night (22:00-05:00, UTC+8), it increased from 2.95% to 15.72%. When the SA-sCIg fraction is large, SA-g also increases to some extent under the modified mechanism. The simulated SA-g exhibits a moderate correlation with online SO_4^{2-} measurements(R=0.54): the model reproduces daytime SO_4^{2-} peak events reasonably well but performs less well at night. Because the SA-sCIg fraction is generally higher at night—where the model simulation performs poorly—the mechanism modification yields a more pronounced improvement in nighttime SA simulations, thereby slightly reducing the model–observation bias.

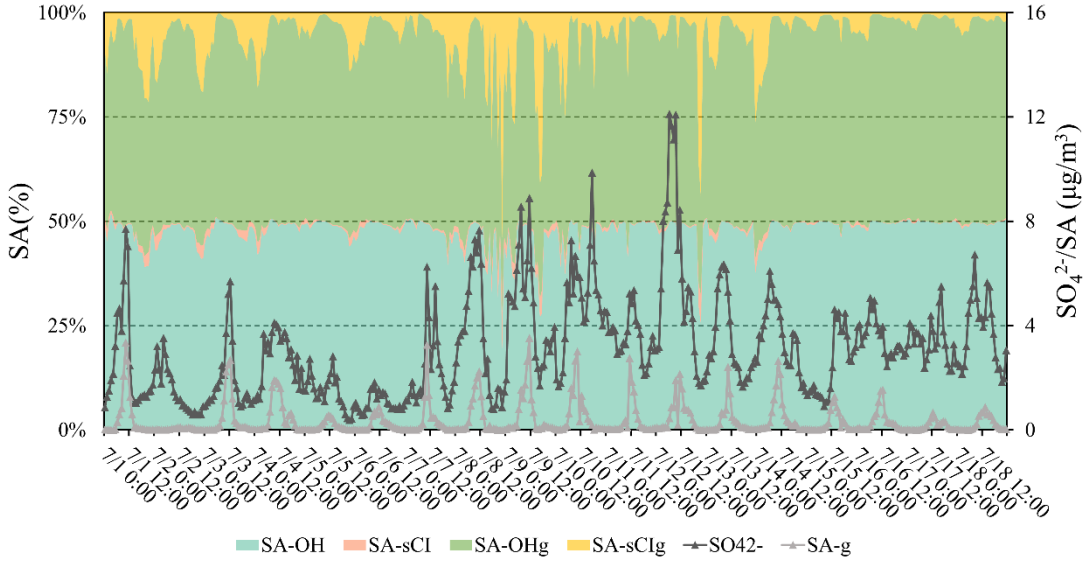

Figure 6. Simulated formation of SA from 2021.07.01 to 2021.07.18 using the AtChem model coupled with MCM v3.3.1 and MCM v3.3.1g.

We trained a random forest (RF) model using long-term observations from September 1, 2019 through June 2022—$PM_{2.5}$, O_3, SO_2, NO_3^-, Fe, alkene, JNO_2, WS, T, RH, NO_x, NO_2%, NO_x×NO_2%, and SO_4^{2-}—and used features' SHAP values to identify the dominant sulfate formation pathways and key drivers. Figure 7a presents the SHAP distributions for all features during 2021.07.01–2021.07.18, ordered by mean |SHAP| value from largest to smallest. The two most influential factors are NO_3^- and SO_2, both exhibiting predominantly positive SHAP values and positive correlations with SO_4^{2-}, indicating that secondary processes dominated sulfate formation during the study period. SHAP values for WS clustered around zero further support this view. T shows mainly large positive SHAP values and a positive correlation with SO_4^{2-}; RH has SHAP values concentrated near zero and shows a slight negative correlation with SO_4^{2-}. Fe exhibits a clear negative contribution to SO_4^{2-}.

https://doi.org/10.5194/egusphere-2025-6276
Preprint. Discussion started: 12 February 2026

Taken together, the roles of T, RH, and Fe indicate that aqueous-phase reactions were not the primary formation pathway during this period. The significant positive contributions of O_3 and alkene underscore the importance of gas-phase pathways; therefore, SO_4^{2-} can serve as a proxy for variations in H_2SO_4.

Using the daytime 5% average SA-sCIg fraction and the nighttime 10% average SA-sCIg fraction as classification thresholds, we split the 2021.07.01 to 2021.07.18 period into separate daytime and nighttime high-sCIs and low-sCIs datasets. For each dataset, we extracted the SHAP values of NO_x, NO_2%, and $NO_x \times NO_2$% and generated a comparative beeswarm plot (Fig. 7b). We find that, both during the day and at night, the high-sCIs datasets feature more negative SHAP values and larger |SHAP| for NO_x and $NO_x \times NO_2$%, indicating a more pronounced negative relationship with SO_4^{2-}. This suggests that, within the high-sCIs datasets, NO_x lowers SO_4^{2-} concentrations; combined with the conclusions of Sect. 3.2, it follows that sCIs% must increase under these conditions. The analysis of SO_4^{2-} observations aligns well with the AtChem-MCM v3.3.1g results, confirming the indispensable role of sCIs in the gas-phase oxidation of SO_2.

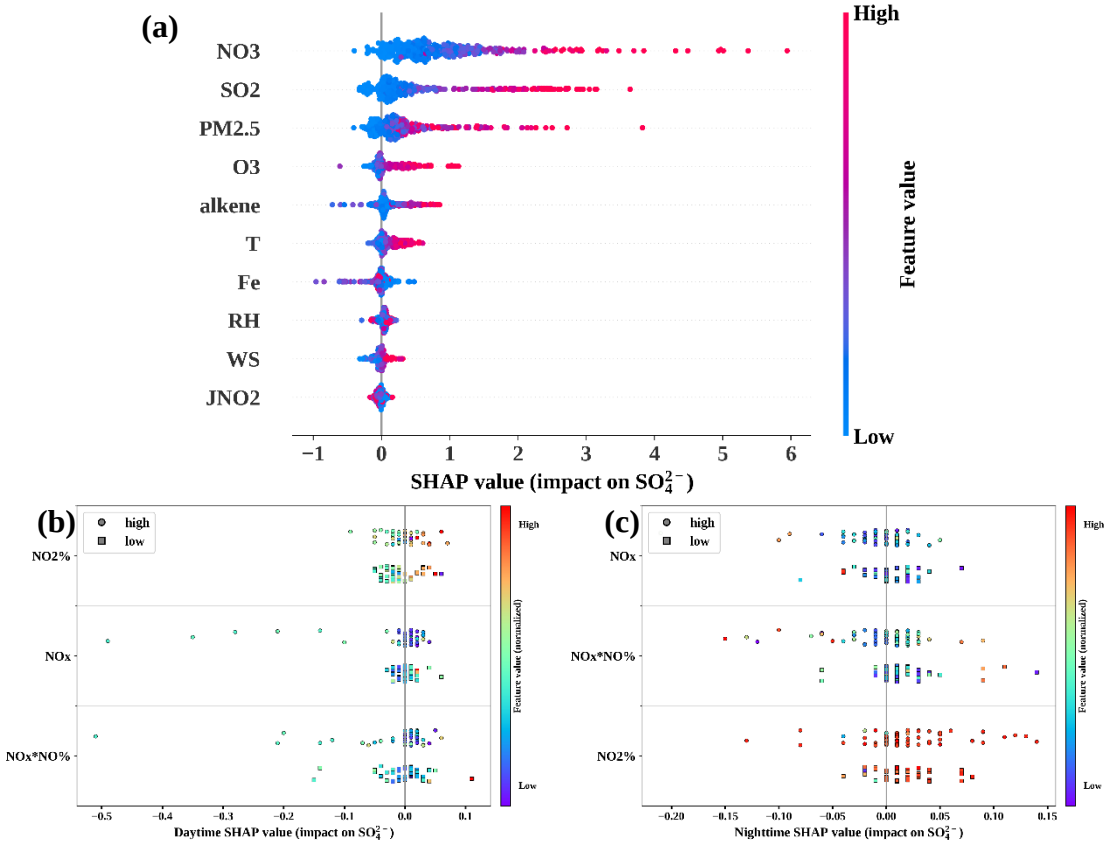

Figure 7. (a) SHAP value distributions for all features during 1–18 July 2021. (b) SHAP value distributions for NO_x, NO_2%, and the $NO_x \times NO_2$% interaction in high-sCIs and low-sCIs datasets, shown separately for daytime and nighttime.

https://doi.org/10.5194/egusphere-2025-6276
Preprint. Discussion started: 12 February 2026

4 Summary and conclusion

In this study, we systematically evaluated the role of stabilized Criegee intermediates (sCIs) in the gas-phase oxidation of SO_2 by combining a box model coupled with the updated Master Chemical Mechanism (MCM v3.3.1g) and machine learning techniques. While the hydroxyl radical (OH) has traditionally been considered the dominant oxidant, our results, based on the latest kinetic data, demonstrate that the contribution of sCIs has been significantly underestimated.

By updating the yield and bimolecular reaction rate coefficients of sCIs, we found that the contributions of precursor species to the sCIs oxidation capacity increased by a factor of 1.97–10.75. Notably, the importance of isoprene rose substantially, becoming the most critical alkene species after updating mechanism. Our sensitivity analysis utilizing the XGBoost model revealed that the atmospheric significance of sCIs is fundamentally governed by the kinetic competition between sCIs and OH radicals. Ozone and alkenes act as the primary synergistic drivers promoting the fractional contribution of sCIs ($\mu_{sCIs\%}$). In addition, another finding of this work is the distinct, diurnal regulatory effect of nitrogen oxides (NO_x) on the competition between sCIs and OH pathways. During the daytime, NO_x primarily modulates the radical propagation cycle; thus, lower NO_x levels favor a higher relative contribution from sCIs. Conversely, at night, NO_x influences the radical termination process. High nighttime NO_x levels suppress the already scarce OH radicals via termination reactions, thereby indirectly amplifying the relative importance of the sCIs pathway. This implies that when NO_x exerts a negative impact on H_2SO_4 formation (via OH suppression), the fractional contribution of sCIs paradoxically increases. Constrained simulations using the AtChem model, focused on a period dominated by gas-phase sulfate formation identified by a Random Forest model, quantified these impacts. The updated mechanism elevated the contribution of sCIs to gas-phase sulfuric acid from 1.11% to 7.13% during the day and from 2.95% to 15.72% at night. These findings suggest that high ozone levels in urban areas, in particular resulting from imbalanced NO_x and VOCs emission reductions, create an ideal environment for sCIs-mediated oxidation. Furthermore, the sCIs pathway becomes particularly indispensable at night when photolysis-driven OH production is absent.

Therefore, a coordinated strategy targeting both VOCs (specifically alkenes) and NO_x is necessary to constrain sCIs-mediated oxidation and effectively reduce sulfate pollution. While our box model simulations offer detailed mechanistic understanding, they are limited by the exclusion of meteorological factors, physical transport processes, and multiphase chemistry. Future studies employing chemical transport models are needed to quantify the role of sCIs in complex air pollution more comprehensively. Given the tightened WHO guidelines specifically for $PM_{2.5}$ and the potential bottlenecks in current emission reduction efforts, pinpointing the specific contributions of sCIs is crucial. This understanding suggests that the sCIs pathway may serve as a key leverage point for designing precise strategies for the synergistic control of $PM_{2.5}$ and ozone.

Data availability

The dataset used in this study is publicly available at: https://doi.org/10.5281/zenodo.17946348.

https://doi.org/10.5194/egusphere-2025-6276
Preprint. Discussion started: 12 February 2026

Supplement link

The link to the supplement will be included by Copernicus, if applicable.

Author contributions

YZ developed the methodology, performed data curation, visualization, formal analysis, and wrote the original draft. QC was responsible for conceptualization, formal analysis, funding acquisition, and reviewed and edited the manuscript. LH and WG participated in the revision of the manuscript. CS, DG, LJ and GY contributed to data curation.

Competing interests

The contact author has declared that none of the authors has any competing interests.

Disclaimer

Copernicus Publications remains neutral with regard to jurisdictional claims made in the text, published maps, institutional affiliations, or any other geographical representation in this paper. While Copernicus Publications makes every effort to include appropriate place names, the final responsibility lies with the authors. Views expressed in the text are those of the authors and do not necessarily reflect the views of the publisher.

Acknowledgements

This research was supported by the Lanzhou science and technology bureau, Project No. 2022-2-15, Research and Development of Key technologies for photocatalysis of low concentration organic waste Gas and the National Natural Science Foundation of China (grant no. 42305118). We thank the editors and anonymous reviewers for their valuable comments on the manuscript. During the preparation of this work, we used ChatGPT to proofread and refine the English expression of the manuscript. This included correcting grammatical errors, enhancing clarity, and improving the overall flow and coherence of the text. After using this tool, we reviewed and edited the content and take full responsibility for the content of the published article.

Financial support

The Lanzhou science and technology bureau, Project No. 2022-2-15, Research and Development of Key technologies for photocatalysis of low concentration organic waste Gas. The National Natural Science Foundation of China (grant no. 42305118).

https://doi.org/10.5194/egusphere-2025-6276
Preprint. Discussion started: 12 February 2026

References

Anon: WHO Global Air Quality Guidelines: Particulate Matter (PM2. 5 and PM10), Ozone, Nitrogen Dioxide, Sulfur Dioxide and Carbon Monoxide, 1st ed., World Health Organization, Geneva, 1 pp., 2021.

Anon: Mauldin Iii 等 - 2012 - A new atmospherically relevant oxidant of sulphur .pdf, n.d.

Breiman, L.: Random Forests, Machine Learning, 45, 5–32, https://doi.org/10.1023/A:1010933404324, 2001.

Cao, J., Qiu, X., Gao, J., Wang, F., Wang, J., Wu, J., and Peng, L.: Significant decrease in SO2 emission and enhanced atmospheric oxidation trigger changes in sulfate formation pathways in China during 2008–2016, Journal of Cleaner Production, 326, 129396, https://doi.org/10.1016/j.jclepro.2021.129396, 2021.

Cao, J., Zheng, B., Chen, J., and Liu, Y.: Assessment of sulfate and nitrate variations in China during 1990 2020: Insights into source contributions and formation pathways, Journal of Hazardous Materials, 489, 137600, https://doi.org/10.1016/j.jhazmat.2025.137600, 2025.

Chen, J.: Long-term exposure to PM and all-cause and cause-specific mortality_ A systematic review and meta-analysis, Environment International, 2020.

Chen, J., Wang, K., Du, P., Zang, Y., Zhang, P., Xia, J., Chen, C., and Yu, Z.: Quantifying the main and interactive effects of the dominant factors on the diurnal cycles of land surface temperature in typical urban functional zones, Sustainable Cities and Society, 114, 105727, https://doi.org/10.1016/j.scs.2024.105727, 2024.

Cox, R. A., Ammann, M., Crowley, J. N., Herrmann, H., Jenkin, M. E., McNeill, V. F., Mellouki, A., Troe, J., and Wallington, T. J.: Evaluated kinetic and photochemical data for atmospheric chemistry: Volume VII – Criegee intermediates, Atmos. Chem. Phys., 20, 13497–13519, https://doi.org/10.5194/acp-20-13497-2020, 2020.

Criegee, R., Blust, G., and Zinke, H.: Eine neuartige Synthese von Ozoniden, Chem. Ber., 87, 766–768, https://doi.org/10.1002/cber.19540870524, 1954.

Dada, L., Ylivinkka, I., Baalbaki, R., Li, C., Guo, Y., Yan, C., Yao, L., Sarnela, N., Jokinen, T., Daellenbach, K. R., Yin, R., Deng, C., Chu, B., Nieminen, T., Wang, Y., Lin, Z., Thakur, R. C., Kontkanen, J., Stolzenburg, D., Sipilä, M., Hussein, T., Paasonen, P., Bianchi, F., Salma, I., Weidinger, T., Pikridas, M., Sciare, J., Jiang, J., Liu, Y., Petäjä, T., Kerminen, V.-M., and Kulmala, M.: Sources and sinks driving sulfuric acid concentrations in contrasting environments: implications on proxy calculations, Atmos. Chem. Phys., 20, 11747–11766, https://doi.org/10.5194/acp-20-11747-2020, 2020.

Dai, Q., Bi, X., Song, W., Li, T., Liu, B., Ding, J., Xu, J., Song, C., Yang, N., Schulze, B. C., Zhang, Y., Feng, Y., and Hopke, P. K.: Residential coal combustion as a source of primary sulfate in Xi'an, China, Atmospheric Environment, 196, 66–76, https://doi.org/10.1016/j.atmosenv.2018.10.002, 2019.

Fatahi, R., Nasiri, H., Dadfar, E., and Chehreh Chelgani, S.: Modeling of energy consumption factors for an industrial cement vertical roller mill by SHAP-XGBoost: a "conscious lab" approach, Sci Rep, 12, 7543, https://doi.org/10.1038/s41598-022-11429-9, 2022.

Friedman, J. H.: Greedy function approximation: A gradient boosting machine., Ann. Statist., 29, https://doi.org/10.1214/aos/1013203451, 2001.

https://doi.org/10.5194/egusphere-2025-6276
Preprint. Discussion started: 12 February 2026

Geng, G., Zheng, Y., Zhang, Q., Xue, T., Zhao, H., Tong, D., Zheng, B., Li, M., Liu, F., Hong, C., He, K., and Davis, S. J.: Drivers of PM2.5 air pollution deaths in China 2002–2017, Nat. Geosci., 14, 645–650, https://doi.org/10.1038/s41561-021-00792-3, 2021.

Gunthe, S. S., Rose, D., Su, H., Garland, R. M., Achtert, P., Nowak, A., Wiedensohler, A., Kuwata, M., Takegawa, N., Kondo, Y., Hu, M., Shao, M., Zhu, T., Andreae, M. O., and Pöschl, U.: Cloud condensation nuclei (CCN) from fresh and aged air pollution in the megacity region of Beijing, Atmos. Chem. Phys., 11, 11023–11039, https://doi.org/10.5194/acp-11-11023-2011, 2011.

Guo, Y., Yan, C., Li, C., Ma, W., Feng, Z., Zhou, Y., Lin, Z., Dada, L., Stolzenburg, D., Yin, R., Kontkanen, J., Daellenbach, K. R., Kangasluoma, J., Yao, L., Chu, B., Wang, Y., Cai, R., Bianchi, F., Liu, Y., and Kulmala, M.: Formation of nighttime sulfuric acid from the ozonolysis of alkenes in Beijing, Atmos. Chem. Phys., 21, 5499–5511, https://doi.org/10.5194/acp-21-5499-2021, 2021a.

Guo, Y., Yan, C., Li, C., Ma, W., Feng, Z., Zhou, Y., Lin, Z., Dada, L., Stolzenburg, D., Yin, R., Kontkanen, J., Daellenbach, K. R., Kangasluoma, J., Yao, L., Chu, B., Wang, Y., Cai, R., Bianchi, F., Liu, Y., and Kulmala, M.: Formation of nighttime sulfuric acid from the ozonolysis of alkenes in Beijing, Atmospheric Chemistry and Physics, 21, 5499–5511, https://doi.org/10.5194/acp-21-5499-2021, 2021b.

Hata, H., Hoshino, S., Fujita, M., and Tonokura, K.: Atmospheric impact of isoprene-derived Criegee intermediates and isoprene hydroxy hydroperoxide on sulfate aerosol formation in the Asian region, Atmospheric Environment: X, 20, 100226, https://doi.org/10.1016/j.aeaoa.2023.100226, 2023.

Jenkin, M. E., Young, J. C., and Rickard, A. R.: The MCM v3.3.1 degradation scheme for isoprene, Atmos. Chem. Phys., 15, 11433–11459, https://doi.org/10.5194/acp-15-11433-2015, 2015.

Khan, M. A. H., Percival, C. J., Caravan, R. L., Taatjes, C. A., and Shallcross, D. E.: Criegee intermediates and their impacts on the troposphere, Environ. Sci.: Processes Impacts, 20, 437–453, https://doi.org/10.1039/C7EM00585G, 2018.

Kukui, A., Chartier, M., Wang, J., Chen, H., Dusanter, S., Sauvage, S., Michoud, V., Locoge, N., Gros, V., Bourrianne, T., Sellegri, K., and Pichon, J.-M.: Role of Criegee intermediates in the formation of sulfuric acid at a Mediterranean (Cape Corsica) site under influence of biogenic emissions, Atmos. Chem. Phys., 21, 13333–13351, https://doi.org/10.5194/acp-21-13333-2021, 2021.

Li, J., Kohno, N., Sakamoto, Y., Fukusaki, Y., Kousa, Y., Sadanaga, Y., Nakashima, Y., Sato, K., Ramasamy, S., Takami, A., Yoshino, A., Nakayama, T., Kato, S., Ono, N., Zhou, J., Bai, Y., and Kajii, Y.: A quantitative understanding of total OH reactivity and ozone production in a coastal industrial area during the Yokohama air quality study (AQUAS) campaign of summer 2019, Atmospheric Environment, 267, 118754, https://doi.org/10.1016/j.atmosenv.2021.118754, 2021.

Li, T., Zhang, Q., Peng, Y., Guan, X., Li, L., Mu, J., Wang, X., Yin, X., and Wang, Q.: Contributions of various driving factors to air pollution events: Interpretability analysis from Machine learning perspective, Environment International, 173, 107861, https://doi.org/10.1016/j.envint.2023.107861, 2023.

Liu, L., Bei, N., Wu, J., Liu, S., Zhou, J., Li, X., Yang, Q., Feng, T., Cao, J., Tie, X., and Li, G.: Effects of stabilized Criegee intermediates (sCIs) on sulfate formation: a sensitivity analysis during summertime in Beijing–Tianjin–Hebei (BTH), China, Atmos. Chem. Phys., 19, 13341–13354, https://doi.org/10.5194/acp-19-13341-2019, 2019.

Liu, S., Wang, G., Kong, F., Zhao, N., Gao, W., and Zhang, H.: PM2.5 pollution characteristics, drivers, and regional transport during different pollution levels in Linyi, China: An integrated PMF-ML-SHAP framework and transport models, Journal of Hazardous Materials, 494, 138534, https://doi.org/10.1016/j.jhazmat.2025.138534, 2025.

https://doi.org/10.5194/egusphere-2025-6276
Preprint. Discussion started: 12 February 2026

Lundberg, S. M., Nair, B., Vavilala, M. S., Horibe, M., Eisses, M. J., Adams, T., Liston, D. E., Low, D. K.-W., Newman, S.-F., Kim, J., and Lee, S.-I.: Explainable machine-learning predictions for the prevention of hypoxaemia during surgery, Nat Biomed Eng, 2, 749–760, https://doi.org/10.1038/s41551-018-0304-0, 2018.

Lyu, Y., Wu, H., Liu, X., Han, F., Lv, F., Pang, X., and Chen, J.: Co-Occurring Extremes of Fine Particulate Matter ($PM_{2.5}$) and Ground-Level Ozone in the Summer of Southern China, Geophysical Research Letters, 51, e2023GL106527, https://doi.org/10.1029/2023GL106527, 2024.

Newland, M. J., Rickard, A. R., Alam, M. S., Vereecken, L., Muñoz, A., Ródenas, M., and Bloss, W. J.: Kinetics of stabilised Criegee intermediates derived from alkene ozonolysis: reactions with SO_2 , H_2 O and decomposition under boundary layer conditions, Phys. Chem. Chem. Phys., 17, 4076–4088, https://doi.org/10.1039/C4CP04186K, 2015a.

Newland, M. J., Rickard, A. R., Alam, M. S., Vereecken, L., Muñoz, A., Ródenas, M., and Bloss, W. J.: Kinetics of stabilised Criegee intermediates derived from alkene ozonolysis: reactions with SO_2 , H_2 O and decomposition under boundary layer conditions, Phys. Chem. Chem. Phys., 17, 4076–4088, https://doi.org/10.1039/C4CP04186K, 2015b.

Orellano, P.: Short-term exposure to particulate matter (PM10 and PM2.5), nitrogen dioxide (NO2), and ozone (O3) and all-cause and cause-specific mortality_ Systematic review and meta-analysis, Environment International, 2020.

Quaas, J., Jia, H., Smith, C., Albright, A. L., Aas, W., Bellouin, N., Boucher, O., Doutriaux-Boucher, M., Forster, P. M., Grosvenor, D., Jenkins, S., Klimont, Z., Loeb, N. G., Ma, X., Naik, V., Paulot, F., Stier, P., Wild, M., Myhre, G., and Schulz, M.: Robust evidence for reversal of the trend in aerosol effective climate forcing, Atmos. Chem. Phys., 22, 12221–12239, https://doi.org/10.5194/acp-22-12221-2022, 2022.

Ren, R., Li, Z., Yan, P., Wang, Y., Wu, H., Cribb, M., Wang, W., Jin, X., Li, Y., and Zhang, D.: Measurement report: The effect of aerosol chemical composition on light scattering due to the hygroscopic swelling effect, Atmos. Chem. Phys., 21, 9977–9994, https://doi.org/10.5194/acp-21-9977-2021, 2021.

Saunders, S. M., Jenkin, M. E., Derwent, R. G., and Pilling, M. J.: Protocol for the development of the Master Chemical Mechanism, MCM v3 (Part A): tropospheric degradation of non-aromatic volatile organic compounds, Atmos. Chem. Phys., 3, 161–180, https://doi.org/10.5194/acp-3-161-2003, 2003.

Shabin, M., Kumar, A., Hakkim, H., Rudich, Y., and Sinha, V.: Sources, sinks, and chemistry of Stabilized Criegee Intermediates in the Indo-Gangetic Plain, Science of The Total Environment, 896, 165281, https://doi.org/10.1016/j.scitotenv.2023.165281, 2023.

Song, X., Yi, J., Chen, Y., Su, Y., Wang, H., Liu, A., Wu, D., and Li, Q.: Condensable particulate matter emissions regulated by flue gas desulfurization technologies in typical industrial plants, Journal of Hazardous Materials, 489, 137527, https://doi.org/10.1016/j.jhazmat.2025.137527, 2025.

Tang, L., Feng, Z., Shang, D., Zeng, L., Wu, Z., Wang, H., Chen, S., Li, X., Zeng, L., Hu, J., and Hu, M.: Ongoing uncoordinated anthropogenic emission abatement promotes atmospheric new particle growth in a Chinese megacity, Nat Commun, 16, 6720, https://doi.org/10.1038/s41467-025-62011-6, 2025.

Wang, T., Xue, L., Feng, Z., Dai, J., Zhang, Y., and Tan, Y.: Ground-level ozone pollution in China: a synthesis of recent findings on influencing factors and impacts, Environ. Res. Lett., 17, 063003, https://doi.org/10.1088/1748-9326/ac69fe, 2022a.

https://doi.org/10.5194/egusphere-2025-6276
Preprint. Discussion started: 12 February 2026

Wang, Y., Du, Y., Fang, J., Dong, X., Wang, Q., Ban, J., Sun, Q., Ma, R., Zhang, W., He, M. Z., Liu, C., Niu, Y., Chen, R., Kan, H., and Li, T.: A Random Forest Model for Daily $PM_{2.5}$ Personal Exposure Assessment for a Chinese Cohort, Environ. Sci. Technol. Lett., 9, 466–472, https://doi.org/10.1021/acs.estlett.1c00970, 2022b.

Wang, Z., Nie, W., Liu, Y., Yang, L., Liu, C., Zhang, Y., Yan, C., Zha, Q., Ge, D., Qi, X., Zhou, C., Chen, L., Zhou, X., Wang, L., Huang, D. D., Chi, X., and Ding, A.: Gaseous Sulfuric Acid Contributions to Sulfate Formation in Urban Atmosphere, Environ. Sci. Technol. Lett., 12, 189–195, https://doi.org/10.1021/acs.estlett.4c01028, 2025.

Yao, L., Garmash, O., Bianchi, F., Zheng, J., Yan, C., Kontkanen, J., Junninen, H., Mazon, S. B., Ehn, M., Paasonen, P., Sipilä, M., Wang, M., Wang, X., Xiao, S., Chen, H., Lu, Y., Zhang, B., Wang, D., Fu, Q., Geng, F., Li, L., Wang, H., Qiao, L., Yang, X., Chen, J., Kerminen, V.-M., Petäjä, T., Worsnop, D. R., Kulmala, M., and Wang, L.: Atmospheric new particle formation from sulfuric acid and amines in a Chinese megacity, Science, 361, 278–281, https://doi.org/10.1126/science.aao4839, 2018.

Ye, C., Lu, K., Song, H., Mu, Y., Chen, J., and Zhang, Y.: A critical review of sulfate aerosol formation mechanisms during winter polluted periods, Journal of Environmental Sciences, 123, 387–399, https://doi.org/10.1016/j.jes.2022.07.011, 2023.

Ye, C., Tan, Z., Li, X., Ma, X., Lu, K., and Zhang, Y.: Persistent Nitrogen Oxide Reductions Unmask Worsening Wintertime Photochemical Pollution in Urban Environments, Environ. Sci. Technol., 59, 17383–17386, https://doi.org/10.1021/acs.est.5c07896, 2025.

Yi, Z. and Wu, L.: Identification of factors influencing net primary productivity of terrestrial ecosystems based on interpretable machine learning --evidence from the county-level administrative districts in China, Journal of Environmental Management, 326, 116798, https://doi.org/10.1016/j.jenvman.2022.116798, 2023.

Zhu, T., Tang, M., Gao, M., Bi, X., Cao, J., Che, H., Chen, J., Ding, A., Fu, P., Gao, J., Gao, Y., Ge, M., Ge, X., Han, Z., He, H., Huang, R.-J., Huang, X., Liao, H., Liu, C., Liu, H., Liu, J., Liu, S. C., Lu, K., Ma, Q., Nie, W., Shao, M., Song, Y., Sun, Y., Tang, X., Wang, T., Wang, T., Wang, W., Wang, X., Wang, Z., Yin, Y., Zhang, Q., Zhang, W., Zhang, Y., Zhang, Y., Zhao, Y., Zheng, M., Zhu, B., and Zhu, J.: Recent Progress in Atmospheric Chemistry Research in China: Establishing a Theoretical Framework for the “Air Pollution Complex,” Adv. Atmos. Sci., 40, 1339–1361, https://doi.org/10.1007/s00376-023-2379-0, 2023.